MICROMACHINED PLANAR INDUCTORS WITH ELECTROPLATED NICKEL-IRON PERMALLOY CORES

(Spiral Type, Solenoid Type, and Toroidal-Meander Type)

Chong H. Ahn and Mark G. Allen *

Center for Microelectronic Sensors and MEMS
Department of Electrical & Computer Engineering
and Computer Science
University of Cincinnati, Cincinnati, OH 45221-0030

* Microelectronics Research Center
School of Electrical and Computer Engineering
Georgia Institute of Technology, Atlanta, GA 30322-0250

ABSTRACT

Three new micromachined planar inductors with electroplated nickel-iron permalloy cores, a spiral type, a solenoid type and a toroidal meander-type, are realized on silicon wafers using micromachining techniques, and their electrical properties are compared. In particular, emphasis is placed on low temperature-CMOS-compatible process, high current carrying capacity, high magnetic flux density, closed magnetic circuits, and low product cost. The realized inductors have shown their suitability for magnetic microelectromechanical systems (MEMS) applications such as micromotors, microactuators, microsensors, and integrated power converters, which envisages new micropower magnetics on silicon wafers with integrated circuits (IC).

INTRODUCTION

In recent years, the demands for new planar micromachined inductors on "a chip" which have high inductance and Q-factor have been greatly increased due to the rapid growth of magnetic driving microelectromechanical systems (MEMS) applications such as magnetic microactuators and microsensors [1-8] and integrated magnetic micropower converter devices [9-11]. In particular, they are usually required to have high current carrying capacity, high magnetic flux density, closed magnetic circuits, and low product cost. The fabrication of the inductive structures in a planar geometry has been understood to be an extremely difficult task, which has been the major obstacle in the implementation of fully integrated and miniaturized magnetic MEMS devices.

Applications of these inductive component have usually been limited due to the relatively low inductance which can be achieved, typically on the order of hundreds of nanohenries (nH) to several microhenries (μH). Thus, most previously fabricated structures have been operated in very high frequency regimes, for instance, as passive components in microwave circuits as well as signal processing circuits [12-18]. Although several inductive thin-film heads [19-21] have been successfully realized for magnetic disk drive systems, the inductive components have also been investigated in focusing not on micropower applications but for signal processing with extremely low noise.

Thus, conventional planar inductors realized to date are usually optimized not for their achievable maximum powers but for their maximum operating frequencies.

However, in recent years, there is a major need for the development of miniaturized planar inductors implemented on "a chip" as a strong magnetic flux generator to produce strong forces for MEMS microactuators as well as to contain large energy for micropower converters. In micro scale, magnetic driving principle has been considered as one of promising principles to produce large forces, since it potentially can overcome drawbacks which would be caused by other driving principles, depending on applications and scales [1-8].

To date, several different types of planar inductors have been proposed and fabricated to address these applications [12-18]. However, most planar inductive components have been fabricated without using a completely closed magnetic circuit, so that leakage flux from the inductor is not negligible. This can be a serious problem in integrating inductors with electronic circuits on the same semiconductor wafers for two reasons: first, magnetic flux interference with an integrated electronic circuit should be suppressed to reduce the magnetic noise in the circuits; and second, a high inductance per unit surface area is desirable in the small area, and any leakage flux produced does not contribute to the total inductance of the device.

Recently, new micromachining MEMS techniques [1-8] have been developed, which promises to revolutionize the conventional concept of magnetic microstructure fabrication. These micromachining techniques provide several approaches for miniaturization of magnetic power components. Cores and conductors of several tens to hundreds of microns in thickness and width with good sidewall and dimensional control can be easily fabricated. Recently by the authors, three types of new micromachined planar inductive components with closed magnetic circuits, a spiral type [22], a solenoid type [23], and a toroidal-meander type inductor [24], have been realized on silicon wafers with electroplated nickel-iron permalloy [25-26] using the micromachining techniques. In particular, emphasis is placed on low temperature-CMOS-compatible fabrication, high current carrying capacity of the fabricated inductive components, high magnetic flux density, closed magnetic circuits, and low product cost.

In magnetic microactuator applications, due to the large core reluctance, the magnetic reluctance due to a small air gap which is inserted in the closed magnetic circuit is usually comparable to the magnetic core reluctance or negligibly small [27]. Thus, the air gap inserted in this geometry may not break the tight flux linkage between the coils and the magnetic circuits, consequently keeping the minimum electro-magnetic field interference (EMI).

In this paper, the electrical characteristics of the three micromachined inductors are compared in terms of inductance, conductor resistance, and Q-factor. Their geometrical effects on electrical properties are also analyzed, and then their potential MEMS applications are discussed depending on their structural as well as electrical characteristics.

STRUCTURE CONCEPTS AND MODELS

Spiral Type Inductor

Several planar spiral inductors have already been reported to date. In these inductors, spiral conductors are placed on an insulated substrate [12-14], a magnetic substrate [15], or between top and bottom magnetic thin films [16]. Due to the geometrical characteristics of the spiral, the generated fluxes without magnetic cores will be spread throughout the surface of the substrate. These fluxes are composed of two components which are either parallel or perpendicular to the surface [14]. Accordingly, it is difficult to guide the magnetic flux to a required point in this structure without using a magnetic core. As one of applications of these inductors, integrated magnetic recording

heads have been investigated since the 1970's. In the magnetic heads, a stack of spiral conductors is deposited on the bottom magnetic core layer, and then top magnetic layers are successively deposited to build magnetic legs, completing a closed magnetic circuit through the gaps [19-21]. However, the magnetic heads have been optimized for non-actuator applications, and may not have high flux generation capability and/or large current carrying capability required for magnetic microactuators. Thus, for magnetic micropower application a new spiral type inductor which is composed of completely closed magnetic circuits and thick conductor lines is introduced.

There are two major restrictions that must be overcome to improve the usefulness of this geometry in micropower applications. First, closed magnetic circuits should be completed using a thick magnetic material with high permeability to reduce magnetic reluctance and to minimize magnetic field interference (making the adhesion of the thick magnetic layer a concern). Second, the spiral conductor should have as small a resistance as possible to reduce power consumption in the conductors. To overcome these limitations, micromachining fabrication techniques are used to build a spiral type inductive component that is composed of completely closed magnetic circuits and thick conductor lines. Spiral inductor structure for this work is shown in Figure 1, where spiral conductor lines are completely encapsulated with an electroplated thick nickel-iron permalloy, thus achieving the closed magnetic circuit.

Simplified models of double spiral coils for the inductance calculation of the closed outer core have been developed [9, 13]. Figure 2 shows a schematic diagram of the inductor which is to be modeled to determine its inductance value. To calculate the mutual inductance, three components of inductance which exists between the i th and j th coils can be defined. If the inductances for path 1, path 2, and internal self-inductance of the coil are defined as L_1, L_2, and L_i respectively, the total inductance L obtained from the summation of these inductances as:

$$L = L_1 + L_2 + L_i . \tag{1}$$

To evaluate an inductance of the spiral type inductor, designed micromachining geometries are substituted into the model. For $a = 1346\ \mu m$, $c = 508\ \mu m$, $d = 30\ \mu m$, $N = 18.5$, $t_m = 8\ \mu m$, and $w = 12.5\ \mu m$, the evaluated values are $L_1 = 14.5\ \mu H$, $L_2 = 10.2\ \mu H$, $L_i = 0.01\ \mu H$, and $L = 24.71\ \mu H$ respectively, where a relative permeability of 800 is assumed. From these calculated values, it is interesting to note that the inductance value resulting from path 2 including the air gaps has an almost comparable value to the inductance value resulting from path 1 through the closed magnetic circuits.

The Q factor of this inductor can be expressed with the spiral conductor resistance of R as:

$$Q = \frac{\omega L}{R} . \tag{2}$$

When the thickness of the conductor lines is increased, the conductor resistance will be reduced. Also, L_1 and L_2 are not greatly affected by the gap variation between the upper core and the lower core which results from the variation of conductor thickness. As a result, the increase in Q-factor resulting from increasing the conductor thickness will be mainly caused by the decrease in the conductor resistance. Thus, the Q-factor increases almost linearly as the thickness of the conductor is increased.

When a planar inductive component is fabricated monolithically with integrated circuits, the area occupied by the planar inductive component must be limited. In a given area (i.e. for the given length of a in this model), the spiral coil turns and resistance are varied as the conductor width (w) is changed. The dimension of the center magnetic core

(i.e. defined as c in this model) also affects the available area which can be occupied by the conductors. Using Equations 1 and 2, Q-factors can be evaluated by changing for the fixed area. It is verified from this evaluation that the Q-factor has larger values in smaller conductor widths, where the inductance value is proportional to the square of the coil turns (i.e. the square of the width variation) but the resistance is linearly proportional to the width variation.

Solenoid Type Inductor

Conventional inductors used in macro scale usually have a solenoid shape, and thus they can be simply fabricated by wrapping coils manually around magnetic cores at macro scale. However, this three dimensional winding structure causes a tremendous difficulty in realizing in planar shape on a wafer. To demonstrate the feasibility of a planar solenoid inductor, solenoid inductive components were fabricated in a hybrid fashion by manually wrapping coils around a magnetic film [28] or an integrated fashion by wrapping coils around an air-core on a silicon substrate [29]. However, the fabrication processes or/and the obtained electrical parameters are not suitable for integrated micromagnetic power device applications. In this work, thus, a new technique is adopted to overcome these limitations using planarization with polyimides and inserting a magnetic bar core in place of the air core. To fabricate this inductor on a planar substrate, quasi-three dimensional micromachining techniques which are compatible with IC processes are required. This planar solenoid type inductor with a closed magnetic circuit can be one of the favorable structure as a magnetic flux generator in micro scale, since the wires wrapped around closed magnetic cores result in low leakage flux and the generated flux can be flexibly guided to the required points. In this work, such structures have been fabricated using multilevel metal schemes to 'wrap' a wire around a magnetic core.

The proposed solenoid type inductor structure is depicted in Figure 3, where the geometry can be thought of as analogous to the conventional toroidal inductor. In this structure, the interconnected metal coils wrap around the magnetic core bar. This type inductive component is considered as one of the more promising inductive components for magnetic micropower device applications, since its geometrical characteristics can meet most of the required conditions of a basic inductive component for magnetic MEMS applications [27].

The metal interconnections used to construct the 'wrapping coils' usually include metal via contacts. These via contacts are another obstacle in the practical applications of this component since they may have a relatively high contact resistance which causes a specific heat dissipation in the via contacts. In achieving a high inductance value, if more turns of solenoid coils are required, more via contacts are added, increasing the total coil resistance. Evaporated metal deposition techniques limit the achievable thickness of a deposited metal and usually cause a high metal contact resistance at the via contacts due to metal oxide or surface contamination resulting from subsequent fabrication processes [30-31]. As a result, when a high current is applied to the conductor coils, heat is generated locally at the via contacts due to their high resistance, resulting in a potential instability problem in this inductive component. Using electroplating techniques, particular efforts have been made to minimize the coil resistance by increasing the thickness of the conductor lines and using electroplated vias. An additional feature of this inductor is that a closed (i.e. toroidal) magnetic circuit is achieved, minimizing the leakage flux and electromagnetic interference, and increasing the inductance value and the Q-factor.

The geometry of the bar-type inductor depicted in Figure 3 can be analogous to the conventional toroidal inductor. Thus, the calculation of inductance for the solenoid

type structure is very simple and more-or-less straightforward. The inductance L of the solenoid inductor structure is expressed as:

$$L = \frac{\mu_0 \mu_r N^2 A_c}{l_c}, \tag{3}$$

where A_c is the cross-sectional area of the magnetic core, l_c is the length of the closed magnetic core, and μ_0 and μ_r are the permeability of the vacuum and the relative permeability of the magnetic core, respectively. To evaluate an inductance of the designed inductor shown in Figure 3, the designed geometries and the measured permeability are substituted into Equation 3. For A_c = 300 μm x 20 μm, l_c = 9000 μm, N = 33 turns, and μ_r = 800, the evaluated inductance value is 0.729 μH.

The Q factor of the inductor can be expressed as:

$$Q = \frac{\omega L}{R} = \frac{\omega \mu_0 \mu_r N A_c A_w}{2W\rho l_c}, \tag{4}$$

where A_w is the cross-sectional area of the conductor, $2W$ is the length of coil per turn, and ρ is the resistivity of the conductor material.

From Equations 3 and 4, it is concluded that inductance and Q factor are linearly proportional to μ_r in the soleniod type inductor as well as the conventional toroidal inductor due to the analogous structure of both inductors.

Toroidal-Meander Type Inductor

In the solenoid type inductor, the conductor lines are wrapped around a magnetic core to form an inductive component. However, by interchanging the roles of the conductor wire and magnetic core in the solenoid inductor, the same effect can be achieved; i.e., a multilevel magnetic core is 'wrapped' around a planar conductor. A new integrated toroidal-meander type inductor can be realized, where toroidal refers to the toroidal core geometry and meander refers to the wrapping approach. This structure has the advantage that a relatively short, planar conductor is used, thus reducing the total conductor resistance. In addition, this geometry has an advantage over the other inductors in realizing microactuators, since the magnetic core is produced on two levels, making it readily available for surface micromachining of movable core actuators.

A schematic drawing of a section of the new integrated toroidal-meander type inductor is shown in Figure 4. This inductor geometry is composed of meander conductor lines located on a simple plane and meander magnetic cores located on the multilevels. Since multilevel meander magnetic cores are interlaced through the center of each meander coil, the magnetic flux density at the center of each meander coil can be calculated by evaluating magnetic fields at the center points, which are generated from the current flowing through all meander conductor elements as shown in Figure 5(a).

By expanding this topology to all distributed meander conductor elements as shown in Figure 5(b), the inductance can be calculated from the total flux linkage (both self and mutual flux linkage) as:

$$L = \frac{\Sigma \Lambda}{I}, \tag{5}$$

where $\Sigma\Lambda$ denotes the total flux linkage, which occurs between the closed multilevel meander magnetic circuit and the flux generated from the current flowing through all meander conductor elements. Note that this relation assumes that the material remains magnetically linear. The z-components of the distributed magnetic flux at these centers are shown in Figure 6. Although at the center of each meander coil, the vector direction of the z-component of the magnetic flux varies from point to point in the opposite direction, all fluxes of z-component in the magnetic circuit flow constructively through the multilevel meander core due to the core geometry. The dimensions of the fully fabricated toroidal-meander type inductor shown in Fig. 4 are as follows: the total inductor size is 4 mm x 1.0 mm; the coil has 30 turns; μ_r is 800; and the cross sectional areas of the magnetic core and the conductor coil are 300 μm x 12 μm and 50 μm x 7 μm respectively. The inductance evaluated from Equation 5 is 0.22 μH.

The Q factor of an inductor can be expressed as:

$$Q = \frac{\omega L}{R} = \frac{\omega \mu_0 \mu_r N A_c A_w}{2(W+L)\rho l_c}, \tag{6}$$

where A_w is the cross section area of conductor, $2(W+L)$ is the length of one meander coil turn, and ρ is the resistivity of conductor material. From Equations 3 through 6, it is concluded that inductance and Q factor are linearly proportional to μ_r in the solenoid type inductor as well as in the toroidal-meander type inductor due to the analogous structure in both inductors. Thus, the introduction of thin film magnetic core in the integrated inductors greatly improve the inductance as well as the Q-factor.

FABRICATION

These three inductive components have very similar fabrication steps. Fabrication process started with oxidized (0.6 μm) 3-inch {100} silicon wafers as a substrate. Onto this substrate, chrome-copper-chrome (300Å / 2000Å / 300Å) was deposited as an electroplating seed layer. In this fabrication, polyimide which is known as a good passivation organic material for integrated circuits was used as a basic insulator, a device molder, and a structure holder, because it has good insulating properties as well as good planarization and mechanical properties. Thick copper or aluminum conductors are plated or deposited, and nickel (81%) - iron (19%) permalloy cores are plated through the defined molds using standard electroplating technique [25, 32-33].

The fabrication steps of spiral inductor are shown in Figure 7. Polyimide was spun and cured on the wafer to build electroplating molds for the bottom magnetic core. Holes were dry-etched in this polyimide and then filled with the nickel/iron permalloy using standard electroplating techniques. For the lower spiral conductor, aluminum was deposited onto the polyimide and patterned using conventional lithography. In order to insulate the conductor line and re-planarize the surface, polyimide was deposited in multiple coats. To connect the lower spiral coils to the upper spiral coils, a via hole was then dry-etched through the polyimide layer. Aluminum or copper was deposited and patterned again for the via and upper spiral coils, composing a double layer spiral conductor. To complete a closed magnetic circuit, magnetic vias were etched both at the center and at the outside of the spiral coils. The magnetic vias were filled with plated nickel-iron permalloy. The top magnetic core was then plated over the magnetic vias, completing the magnetic circuit. Bonding pads were then opened through polyimide layers for the electrical test. The fabricated spiral type inductor has the size of 3 mm x 3

mm x 150 μm having 36 turns of spiral coil. The photomicrograph of the fabricated spiral inductive components with or without an encapsulating magnetic core are shown in Figure 8. Figure 9 shows scanning electron micrograph of the fabricated spiral inductor.

The brief fabrication processes of the solenoid type inductor is shown in Figure 10. The seed layer for bottom conductors was patterned to form the tie bars to be removed after serving as the seed layer for the conductor plating. The cavity to contain the magnetic core bar was dry-etched. The copper conductors and nickel/iron permalloy were plated through the defined molds using standard electroplating techniques. Most fabrication procedures are very similar to those of the spiral type inductor, except electroplated conductors. Figure 11 shows the photomicrograph of the fully fabricated device. The size of fabricated structure is 4 mm x 1.0 mm x 120 μm having 33 turns of multilevel coils. The scanning electron micrograph of the structure is shown in Figure 12, which was taken after dry-etching of the polyimide.

The fabrication processes of the toroidal-meander type inductor is also depicted in Figure 13. This meander geometry has no electrical vias that add resistance to the conductor coil, since the conductor is located in a single plane. Most fabrication procedures are also very similar to the spiral type as well as the solenoid type inductor. The fabricated inductor size is 4 mm x 1.0 mm x 130 μm, which has 30 turns. Figure 14 shows scanning electron micrographs of the fabricated toroidal & meander-type inductor. Note the magnetic via connecting the top and bottom cores in the meander topology.

Finally, all samples were diced into chips for bonding and test.

DEVICE PERFORMANCE AND DISCUSSION

From a typical 36-turn spiral type inductor of 3 mm x 3 mm in area, an inductance of approximately 20 μH was measured at 10 KHz. A plot of inductance versus frequency for two planar spiral type inductor structures, one with a magnetic core and the other without a magnetic core, is shown in Figure 15. The magnetic core has increased the inductance by a factor of 4-5 compared with the structure without the magnetic cores. The obtained inductance of 2.2 $\mu H / mm^2$ at 10 KHz is one of the highest inductance values which has been achieved in an integrated planar inductive component, corresponding to a core permeability of approximately 800. It should be noted that the increase in inductance falls off at frequencies above 3 MHz, presumably due to the decreasing permeability of the nickel-iron permalloy at higher frequencies. The evaluated inductance for this fabricated inductor was 24.71 μH. Thus, the measured and the evaluated inductances are matched well at low frequencies. The measured conductor resistance was approximately 300 ohms. The achieved Q-factor at frequencies around 1 MHz is approximately 0.25. However, in realizing an actual magnetic microactuator using the spiral inductor with magnetic cores, the highest Q factor may not be as important as the lowest conductor resistance. In order to evaluate the capacitance of the inductor, an equivalent circuit was assumed as shown in Figure 16, and the resistance and stray capacitance of the inductor were derived from the measured impedance and phase as a function of frequency using equivalent circuit analysis. From this analysis for a typical 36-turn device 3 mm x 3 mm inductor, the stray capacitance was shown to be in the several 10s of pF, and also shown to have a negligibly small effect over the low frequency ranges used. If a small air gap is introduced between the top core and the center core pole, magnetic force can be generated at the air gap when a current is applied to the spiral coils. Fortunately, air gaps and movable mechanical structures can be easily

inserted as part of the magnetic circuit in this structure by using surface micromachining techniques and sacrificial layers. Thus, this spiral type inductor implemented on a chip can serve as an inductive component in realizing magnetic integrated circuits or modules such as filters, microsensors, DC/DC converters, microvalves, and micropumps.

For a solenoid type inductor of 4 mm x 1.0 mm x 120 μm thickness having 33 turns of multilevel coils, the achieved inductance was approximately 0.4 μH at low frequencies of approximately 10 KHz. The variation of the inductance with frequency is shown in Figure 17. As evaluated in the previous section, the evaluated inductance for this fabricated inductor was 0.729 μH. The measured and the evaluated inductances are also matched well at low frequencies. The measured resistance of the conductor lines was approximately 0.3 ohms. The conductor resistance evaluated from its geometry was approximately 0.308 ohms using a literature value for conductivity of plated copper [30]. Although it was difficult to measure a via contact resistance individually, it was verified from the comparison between the measured and the estimated values that the resistance of a metal via contact had an almost negligible value. Thus, the electroplating technique eliminated via contact instability or high contact resistance problems potentially resulting from unfavorable metal via contacts. The evaluated Q-factor at 1 MHz was approximately 1.5, whose relatively higher value compared with the spiral type would be mainly due to its low conductor resistance. The stray capacitance was shown to be in the *p*F region, and thus it gives a negligibly small effect over the frequency ranges used. The effect of the inductance falloff at higher frequencies shown in Figure 17 is due almost entirely to the dependence of the permeability of the iron-nickel core on frequency. Since this inductive component has favorable magnetic characteristics as well as electrical properties, it is potentially very useful as a basic inductive component in applications for magnetic microsensors, micromotors, electron beam steering lenses, and micromagnetic power devices such as a DC/DC converter.

The fabricated toroidal meander type inductor of 4 mm x 1.0 mm x 130 μ*m*, in size has 30 coil turns. The cross sectional areas of the magnetic core and the conductor coil are 300 μ*m* x 12 μ*m* and 50 μ*m* x 7 μ*m* respectively. The measured inductance values were plotted in Figure 18, which shows a fairly flat response through a frequency of 10 Mhz. At a frequency of 5 Mhz, an inductance of 30 nH / mm^2 was achieved. The evaluated inductance for this fabricated inductor was 0.22 μH, and thus the measured and the evaluated inductances also show fairly good match at low frequencies. The stray capacitance was shown to be in the *pF* region. With the measured inductance and resistance as a function of frequency, the Q value of the device can be estimated from Equation 6. The Q-value at a frequency of 1 Mhz is approximately unity. Several approaches such as increased conductor thickness (to lower the series resistance) or increased core permeability could be taken to increase the Q-factor. The toroidal-meander type inductor implemented on a chip or as an integral part imbedded in the interconnections of a multichip module has already been used as an inductive component in realizing magnetic integrated circuits or modules such as microactuators [34-36], DC/DC power converters [37], or bio-medical applications [38].

Finally, the measured inductances for the micromachined three inductors are plotted in Figure 19 and their electrical parameters are listed in Table I.

CONCLUSIONS

In this work, three new micromachined planar inductors, a spiral, a solenoid and a toroidal-meander type, have been realized on silicon wafers using micromachining and

multilevel metal fabrication techniques. Their electrical and geometrical properties are compared for magnetic microelectromechanical systems (MEMS) applications. In particular, emphasis is placed on low temperature-CMOS-compatible process, high current carrying capacity, high magnetic flux density, closed magnetic circuits, and low product cost. The realized inductive components have shown their suitability for magnetic micropower applications such as magnetic micromotors, magnetic microactuators, microsensors, magnetic particle separators, and miniaturized DC/DC converters, which envisages new micropower magnetics on silicon wafers with integrated circuits (IC).

ACKNOWLEDGMENTS

This work was supported in part by the National Science Foundation under grant ECS-9117074. The authors would like to gratefully acknowledge DuPont and OCG Microelectronic Materials for their donations of polyimide and Lake Shore Cryotronics, Inc. for their assistance in measurements of the magnetic properties of the permalloy thin films. The fabrication was performed in Microelectronics Research Center at the Georgia Institute of Technology.

REFERENCES

[1] K. Yanagisawa and A. Tago and T. Ohkubo and H. Kuwano, Proc. 4th IEEE Workshop on Microelectromechnical Systems, pp. 120-124, Nara, Japan, 1991.
[2] H. Guckel and K. J. Skrobis and T. R. Christenson and J. Klein and S. Han, B. Choi and E. G. Novell and T. W. Chapman, J. of Micromechanics and Microengineerings, Vol. 1, no. 4, pp. 135-138, 1991.
[3] B. Wagner, M. Kreutzer, and W. Benecke, Proc. IEEE Microelectromechanical Systems Workshop, pp. 183-189, 1992.
[4] C. H. Ahn and M. G. Allen, Proc. IEEE Solid-State Sensor and Actuator, pp. 14-18, 1992.
[5] I. J. Busch-Vishniac, Sensors and Actuators, Vol. A. 33, pp. 207-220, 1992
[6] C. Liu, T. Tsao, Y. C. Tai, and C. M. Ho, Proc. IEEE Microelectromechanical Systems Workshop, pp. 57-62, 1994.
[7] J. W. Judy, R. S. Muller, and H. H. Zappe, Solid-State Sensor and Actuator Workshop, pp. 43-48, 1994.
[8] B. Rogge, J. Schulz, J. Mohr, A. Thommes, and W. Menz, Proc. The 8th International Conference on Solid-State Sensors and Actuators, pp. 320-323, 1995.
[9] M. Kimura, N. Miyakoshi, and M. Diabow, Proc. IEEE Microelectromechanical Systems Workshop, pp. 227-232, 1991.
[10] M. Mino, T. Yachi, A. Tago, K. Yanagisawa, and K. Sakakibara, IEEE Transactions on Magnetics, Vol. 28, No. 4, pp. 1969-1973, 1992.
[11] C. H. Ahn, Y. J. Kim, and M. G. Allen, Transducers, 6th International Conference on Solid-State Sensors and Actuators, pp. 70-73, 1993.
[12] A. Olivei, IEEE Trans. on Part, Materials and Packaging, Vol. PMP-5, No. 2, pp. 71-88, 1969.
[13] H. M. Greenhouse, IEEE Trans. on Part, Hybrids and Packaging, Vol. PHP-10, No. 2, pp. 101-109, June 1974
[14] R. Rodriguez, J. M. Dishman, F. D. Dickens, and E. W. Whelan, IEEE Trans. on Components, Hybrids, and Manufacturing Technology, Vol. CHMT-3, No. 4, pp. 535-541, 1980.
[15] W. A. Roshen and D. E. Turcotte, IEEE Trans. on Magnetics, Vol. 24, No. 6, pp. 3213-3216, Nov. 1988.

[16] O. Oshiro, H. Tsujimoto, and K. Shirae, IEEE Trans. on Magnetics, Vol. MAG-23, No. 5, pp. 3759-3761, 1987.
[17] K. Kawabe, H. Koyama, and K. Shirae, IEEE Trans. Magn., vol. MAG-20, pp. 1804-1806, 1984.
[18] M. Yamaguichi, M. Matsumoto, H. Ohzeki, and K. I. Arai, IEEE Trans. Magn, vol. MAG-26, pp. 2014-2016, 1990.
[19] L. T. Romankiw, Proc. The Symposium on Magnetic Materials, Processes, and Devices, The Electrochemical Society, Vol. 90-8, pp. 39-53, 1990.
[20] Y. Miura, T. Takahashi, F. Kume, J. Toda, S. Tsutsumi, and S. Kawakami, IEEE Trans. on Magnetics, Vol. MAG-16, No. 5, pp. 779-881, 1980.
[21] Y. Noro, I. Ohshima, M. Saito, M. Yamada, and K. Tanaka, J. Appl. Phys., Vol. 53, No. 3, pp. 2611-2613, Mar. 1982.
[22] C. H. Ahn and M. G. Allen, Journal of Micromechanics and Microengineering, Vol. 3, pp. 1-9, 1993.
[23] C. H. Ahn, Y. J. Kim, and M. G. Allen, IEEE Transactions on Components, Hybrids, and Manufacturing Technology, Vol. 25, No 3, pp. 356-403, 1994.
[24] C. H. Ahn and M. G. Allen, IEEE Transactions on Magnetics, Vol. 30, No. 1, pp. 73-79, 1994.
[25] R. L. Anderson, E. E. Castellani, P. M. McCaffrey, and L. T. Romankiw, United States Patent #4,003,768.
[26] A. B. Frazier, C. H. Ahn, and M. G. Allen, Sensors and Actuators, Vol. A-45, pp. 47-55, 1994.
[27] C. H. Ahn, Ph.D. Dissertation, Georgia Institute of Technology, Atlanta, GA,
[28] R. F. Soohoo, IEEE Transaction on Magnetics., Vol. MAG-15, pp. 1803-1805, 1979.
[29] S. Kawahito, Y. Sasaki, M. Ashiki, and T. Nakamura, Transducers, 6th International Conference on Solid-State Sensors and Actuators, pp. 1077-1080, 1991.
[30] R. Jensen, J. Cummings, and H. Vora, IEEE Trans. on CHMT, Vol. 7, No. 4, pp. 384-393, 1990.
[31] N. Iwasaki and S. Yamaguchi, IEEE Trans. on CHMT, Vol. 13, No. 2, pp. 440-443, 1990.
[32] I. W. Wolf, Journal of Applied Physics, Vol. 33, No. 3, pp. 1152-1159, 1962.
[33] M. E. Henstock and E. S. Spencer-Timms, Proc. 6th International Metal Finishing Conference, pp. 179-185, 1963.
[34] C. H. Ahn and M. G. Allen, IEEE/ASME Journal of Microelectromechanical Systems (MEMS), Vol. 2, No. 1, pp. 15-22, 1993.
[35] C. H. Ahn and Y. J. Kim, and M. G. Allen, IEEE/ASME Journal of Microelectromechanical Systems (MEMS), Vol. 2, No. 4, pp. 165-173, 1993.
[36] C. H. Ahn and M. G. Allen, Proc. IEEE Microelectromechanical Systems (MEMS) Workshop, Amsterdam, Netherland, pp. 408-412, January 30 - February 2, 1995.
[37] C. H. Ahn and M. G. Allen, IEEE Trans. on Power Electronics, 1994, accepted for publication.
[38] C. H. Ahn and M. G. Allen, Proc. IEEE Microelectromechanical Systems (MEMS) Workshop, pp. 35-41, Japan, January 25-28, 1994.

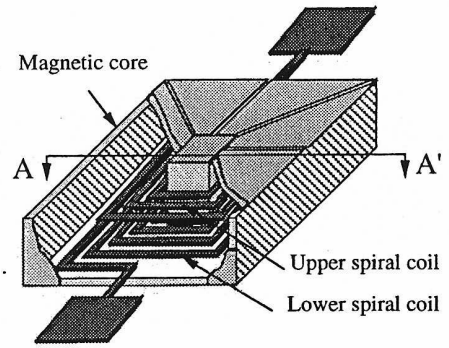

Figure 1. Schematic diagram of a spiral type inductive structure which has a closed magnetic circuit.

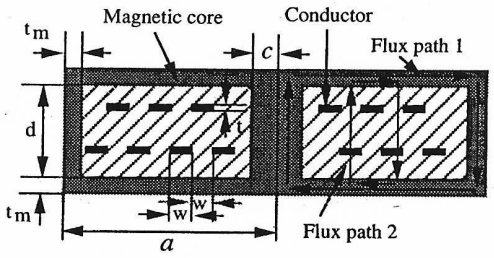

Figure 2. Schematic diagram of spiral inductor to be modeled.

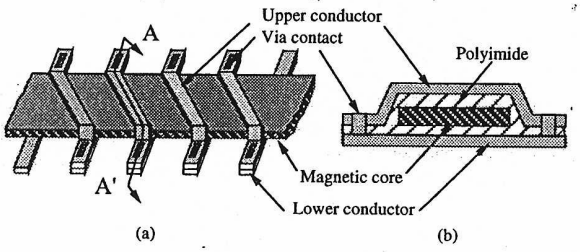

Figure 3. Schematic diagram of the solenoid type inductive component: (a) schematic view; (b) A-A' cut view.

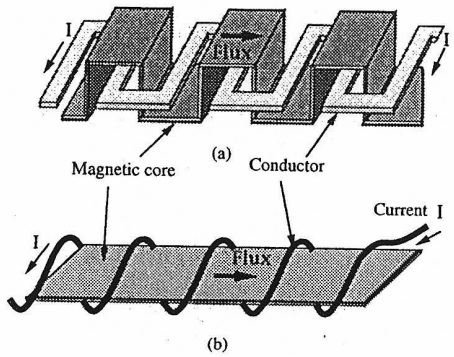

Figure 4. Schematic diagrams of the toroidal-meander type inductor. The structure of the two inductor schemes is analogous: (a) toroidal-meander type inductor; (b) solenoid type inductor.

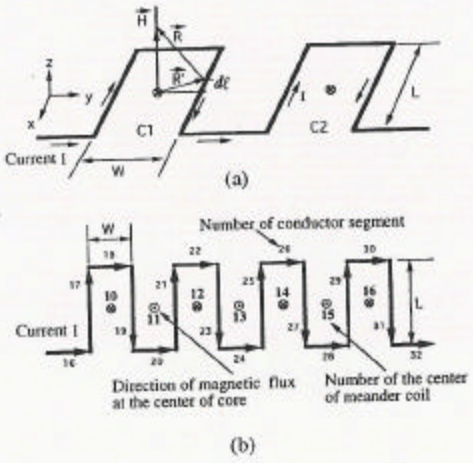

Figure 5. Meander conductor models: (a) coordinate and meander elements for the Biot-Savart law calculation; (b) model of meander conductor including the direction of magnetic flux.

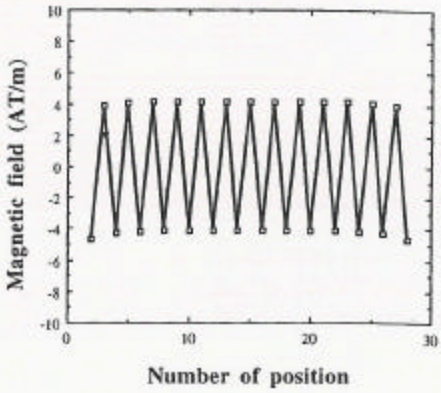

Figure 6. Magnetic field distributions at the center of each meander coil with an assumed current of 1 mA flowing through the conductors. The positive and the negative signs of magnetic field indicate the directions of magnetic field at Z-axis.

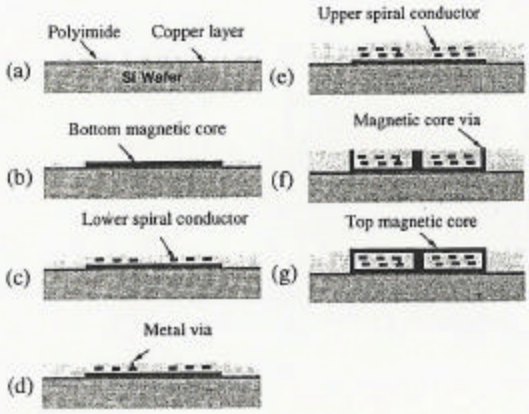

Figure 7. Fabrication sequence of the planar-spiral inductive component.

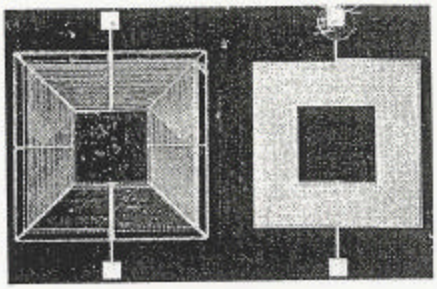

Figure 8. Photomicrograph of the inductive components with (left side) or without (right side) a magnetic core.

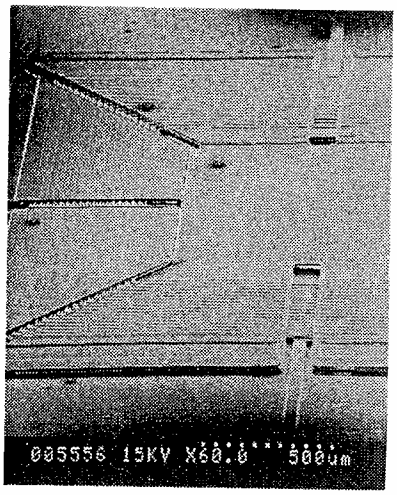

Figure 9. Scanning electron micrograph of the fabricated spiral type inductor.

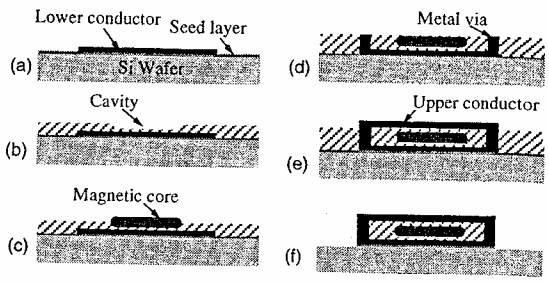

Figure 10. Fabrication steps of the solenoid type inductive component.

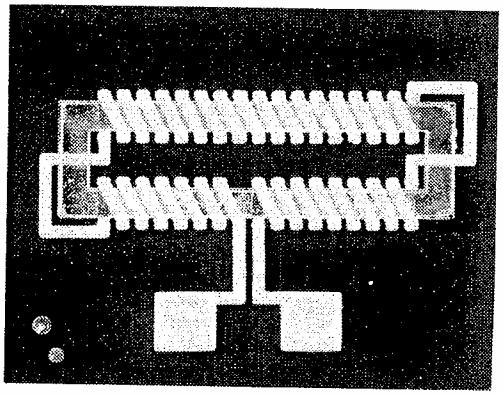

Figure 11. Photomicrograph of the fabricated solenoid type inductor.

Figure 12. Scanning electron micrograph of the fabricated solenoid type inductor.

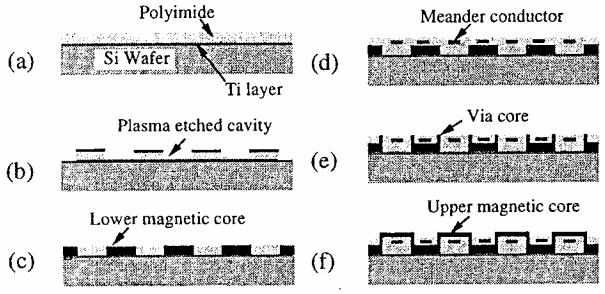

Figure 13. Fabrication sequence of the toroidal-meander type inductor.

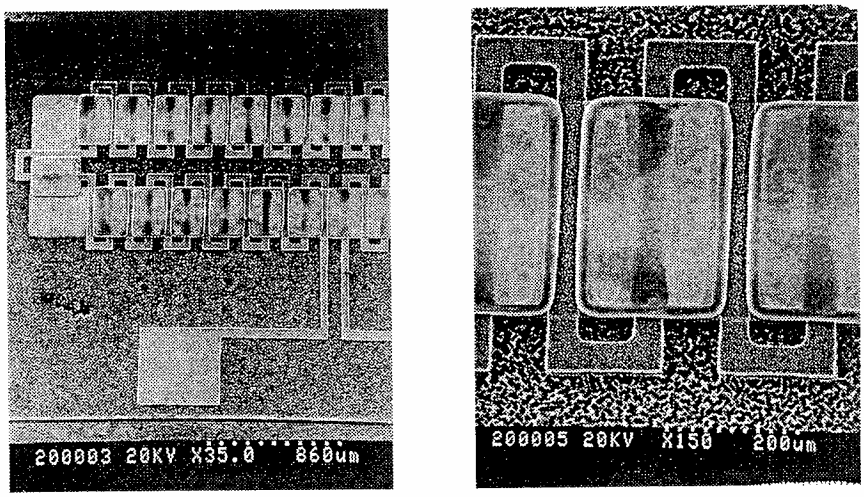

(a) (b)

Figure 14. Scanning electron micrograph of the fabricated toroidal-meander type inductor: (a) half of the inductor; (b) detailed view.

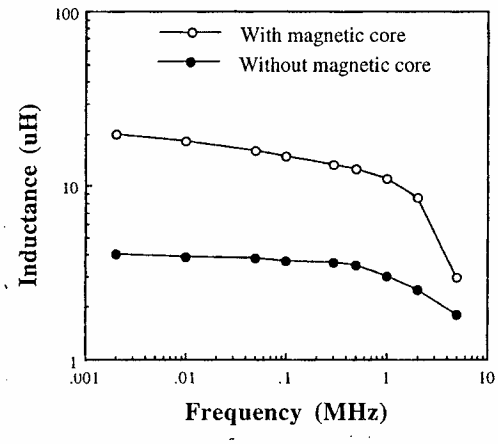

Figure 15. Measured inductance of the spiral type inductor.

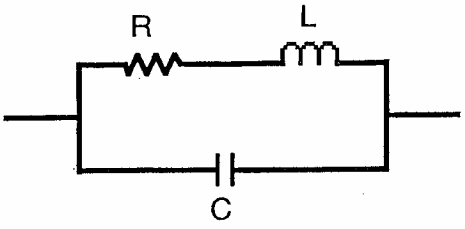

Figure 16. Equivalent circuit of the spiral type inductor.

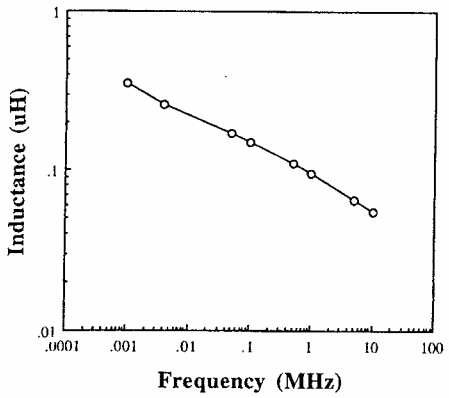

Figure 17. Measured inductance of the solenoid type inductor.

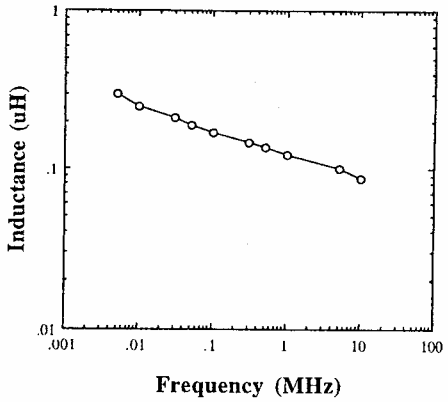

Figure 18. Measured inductance of the toroidal-meander type inductor.

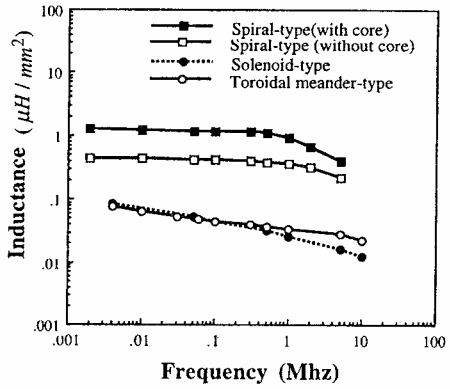

Figure 19. Measured inductance per area ($\mu H / mm^2$) for the three micromachined inductors.

Table I. Electrical parameters of the micromachined inductors

Inductor Type	Inductance ($\mu H / mm^2$) (at 10 KHz)	Resistance (Ω / mm^2)	Capacitance (F)	Q-factor (at 1 MHz)
Spiral Type	1.3	5.6	approximately pF	0.25
Solenoid Type	0.1	0.1	approximately pF	1.5
Toroidal-Meander Type	0.05	0.06	approximately pF	1.0